Sensor-Based Flow Pattern Detection—Gas–Liquid–Liquid Upflow Through a Vertical Pipe

Tanumoy Mukherjee, Gargi Das, and Subhabrata Ray
Dept. of Chemical Engineering, Indian Institute of Technology Kharagpur, Kharagpur 721302, India

Flow distribution during gas–liquid–liquid upflow through a vertical pipe is investigated. The optical probe technique has been adopted for an objective identification of flow patterns. The probability density function (PDF) analysis of the probe signals has been used to identify the range of existence of the different patterns. Dispersed and slug flow have been identified from the nature of the PDF, which is bimodal for slug flow and unimodal for dispersed flow. The water continuous, oil continuous, and emulsion type flow distributions are distinguished on the basis of the PDF moments. The method is particularly useful at high flow rates where visualization techniques fail. Based on this, a flow pattern detection algorithm has been presented. Two different representations of flow pattern maps have been suggested for gas–liquid–liquid three phase flow. © 2014 American Institute of Chemical Engineers *AIChE J*, 60: 3362–3375, 2014*
Keywords: gas–liquid–liquid flow, flow pattern, optical probe, PDF analysis, ternary flow pattern map

Introduction

Gas–liquid–liquid three-phase flow is commonly encountered in oil and gas industry. Gas pipelines often contain water and hydrocarbon condensate and oil pipelines contain water and vapor. There is significant increase in water production during the later stages of a well and water is emitted along with oil and natural gas. Moreover, it is common practice to pump water or steam during secondary and tertiary recovery stages in oil fields. The methods used namely water flooding and gas lift result in simultaneous flow of water, oil, and natural gas, that is, a three-phase mixture. For an efficient design of transport pipelines, it is necessary to know the flow distribution under different flow conditions. Further, the wetting characteristic of oil and water in presence of gas is important to ensure a long life of the pipeline since the relative motion between pipe material and fluid affects the protective layer at the wall and causes erosion of pipeline and associated equipment. Apart from oil and gas recovery, simultaneous gas–liquid–liquid flow occurs during the flow of two immiscible liquids with one of them evaporating/condensing or when two immiscible liquids react to release a gaseous component and all three flows simultaneously through the reactor.

For any multiphase flow system, knowledge of the existing flow pattern is necessary to estimate the hydrodynamics and heat and mass transfer characteristics of the mixture. Several techniques based on radiation attenuation, electrical impedance, photographic analysis, and so forth have been adopted to identify the flow distributions under different flow conditions. These objective methods have primarily been used for two-phase (gas–liquid and liquid–liquid) systems. For three-phase gas–liquid–liquid flow, the majority of the studies (Table 1) have used visual and photographic observations to identify flow patterns. The only exceptions are Wang et al.[4] who have adopted the conductivity probe technique and Piela et al.[10] who have investigated three-phase dispersed flow in a horizontal pipe from signals obtained from a single tip optical fiber probe.

The conventional approach to model three-phase flow has been either to approximate the flow as a two-phase oil–gas system neglecting the water phase or combining oil and water into a single phase and considering the system as a two-phase mixture comprising gas and pseudosingle phase liquid (Tek[15], Oddie et al.[13]). Both the approaches are limited to certain flow conditions and cannot be extended over the entire range of operation. Table 1 also shows that the majority of the studies have been confined to horizontal pipes. Not much is known about gas–liquid–liquid three-phase flows through vertical conduits. One of the earliest work dates back to Woods et al.[1] who experimented on vertical cocurrent oil/water/air upflow in a 0.026 m inner diameter (ID) pipe. They identified nine flow regimes by visual/video observations and pressure measurement techniques and studied the influence of input liquid and gas flow rates as well as flow pattern on holdup. They proposed relations to determine the transition between oil and water dominated regimes. Descamps et al.[2,3] studied the influence of gas injection on phase inversion of oil–water vertical flow. They observed that gas injection does not significantly change the critical concentration of oil and water because the dispersed (oil–water) phase has a strong influence on bubble size. Wang et al.[4] identified oil–water–gas three-phase flow patterns in a vertical pipe on the basis of two kinds of signal measured from mini conductance probe array and vertical multielectrode array. They have constructed six flow pattern

Correspondence concerning this article should be addressed to G. Das at gargi@che.iitkgp.ernet.in.

Table 1. A Survey of Past Experimental Works on Three-Phase Flow

Author (year)	Diameter (m)	Length (m)	Pipe Material	Oil Physical Properties (kgm⁻³,mPas)	Phase Velocity (U_{si}) or Mixture Velocity (U_m) (m/s)	Flow Direction	Brief Description of Work
Woods et al.[1] (1998)	0.026	4.49	Perspex	$\rho = 829$ $\mu = 12.02$ at 20°C	Max $U_{sA} = 37.68$ Max $U_{sW} = 0.28$ Max $U_{sO} = 0.19$	Vertical upward	Identified nine flow regimes Identified the influence of input liquid and gas flow rates and flow pattern on holdup and pressure drop.
Descamps et al.[2] (2006)	0.0828	15.5	SS AISI-316L	$\rho = 830$ $\mu = 7.5$ at 40°C	Max. liquid velocity = 6	Vertical upward	Influence of gas injection on phase inversion Effect of bubble size on pressure drop and critical concentration at phase inversion
Descamps et al.[3] (2007)	0.05	7	Perspex and PVC	$\rho = 794$ $\mu = 3.1$ at 40°C	Max. liquid velocity = 1.8	Vertical upward	Influence of gas injector (bubble size) on efficiency of gas lifts technique.
Wang et al.[4] (2010)	0.125	6	Plexiglass	$\rho = 856$ $\mu = 11.984$ at 40°C	Liquid $U_m = 0.0188$–0.0754 $U_{sA} = 0.00754$–0.17	Vertical upward	Identified six flow pattern using conductance probe. Investigated nonlinear dynamical characteristics of different flow pattern by method of attractor morphological description.
Acikgoz et al.[5] (1992)	0.019	5.78	Plexiglass	$\rho = 864$ $\mu = 116.4$ at 25°C	$U_{sA} = 0.15$–50 $U_{sW} = 0.004$–0.66 $W_{sO} = 0.043,0.09,$ 0.24	Horizontal cocurrent	Identified ten flow regimes classified into two groups i.e water based and oil based.
Stapelberg et al.[6] (1994)	0.0238, 0.059	35	Perspex	$\rho =858$ $\mu = 31.0$ at 25°C	Liquid $U_m = 0.226$–0.244	Horizontal cocurrent	Explained the influence of second immiscible liquid on gas liquid–liquid flow by predicting the slug frequency and pressure drop
Spedding et al.[7] (2005)	0.0259, 0.0501	7.7, 12.52	Perspex	$\rho = 828.5,854.2$ $\mu = 12.2, 39.5$ at 24°C	$U_{sA} = 10$–31 Liquid $U_m = 0.025$–0.051	Horizontal cocurrent	They observed twelve oil dominated flow patterns and ten number of water dominated flow patterns. The flow pattern mapping technique they proposed can predict basic flow regimes for both two and three phase flow.
Wegmann et al.[8] (2007)	0.0056, 0007	5	Glass	$\rho = 818.5$ $\mu = 45$ at 20°C	$U_{sA} = 0.2$–6.77, 0.2–4.33 $U_{sW} = 0.1$–2.0, 0.04–1.3 $U_{sO} = 0.1$–1.0	Horizontal cocurrent	Observed six types of flow patterns by high speed photography with laser induced fluorescence. Discussed the influence of pipe diameter on transition of flow pattern through millimeter pipes.

TABLE 1. (Continued)

Author (year)	Diameter (m)	Length (m)	Pipe Material	Oil Physical Properties (kgm^{-3}, mPas)	Phase Velocity (U_{si}) or Mixture Velocity (U_m) (m/s)	Flow Direction	Brief Description of Work
Bannwart et al.[9] (2009)	0.0284, 0.01	5.43,1	Glass	$\rho = 970$ $\mu = 3400$ at 20°C	$U_{sA} = 0.03$–10 $U_{sW} = 0.04$–0.5 $U_{sO} = 0.01$–2.5	Vertical/horizontal cocurrent	Identified nine water dominated flow patterns for horizontal flow and four water dominated flow patterns for vertical upward flow. Considered the effect of scaling and inclination on flow patterns. Large scale onshore flow experiment carried out and pressure gradient data reported.
Piela et al.[10] (2009)	0.016	26.5	Perspex	$\rho = 794.$ $\mu = 3.0966$ at 20°C	$U_m = 1$–4 m/s	Horizontal	Explained that both bubble size and drop volume fraction has considerable effect of pressure drop as well as flow pattern transition especially at phase inversion
Poesio et al.[11] (2009)	0.021, 0.028, 0.04	9,10	Glass	$\rho = 886,$ $\mu = 1200,900$ at 20°C	$U_{sA} = 0.29, 0.06$–4 $U_{sW} = 0.1$–2.6, 0.04–0.67 $U_{sO} = 0.03$–0.7, 0.46–1.08	Horizontal cocurrent	Provide a database for pressure drop for three phase flow Proposed a model incorporates two fluid model for liquid–liquid flow in Lockhart Martinelli model for the computation of overall pressure drop.
Chen et al.[12] (1999)	0.039	4.32, 6.76	Plexiglass	$\rho = 871$ $\mu = 132.084$ at 20°C	$U_{sA} = 0.45$–19.02 $U_{sW} = 0.018$–1.85 $U_{sO} = 0.014$–0.091	Horizontal helical coil	Observed four flow patterns Proposed a criterion for flow pattern transition in terms of non dimensional parameter and obtained correlation for pressure drop
Oddie et al.[13] (2003)	0.15	11	Plexiglass	$\rho = 810$ $\mu = 1.5$ at 18°C	$U_{sA} = 0.0786$–0.786 $U_{sW} = 0.0314$–0.629 $U_{sO} = 0.0314$–0.629	Inclined pipe (0° to 92°)	Investigated both two phase and three phase flow patterns. Obtained hold up data for steady state and transient flows
Spedding et al.[14] (2008)	0.026	8.1	Perspex	$\rho = 829$ $\mu = 12.0255$ at 20°C	Max $U_{sA} = 37.68$ Max $U_{aW} = 0.282$ Max $U_{sO} = 0.188$	Horizontal 90° elbow bend	Observed significant difference in flow pattern as well as pressure drop in tangent lengths as compare to straight pipe

maps under four total mixture liquid flow rates and reported that an increase in the ratio of oil fraction in liquid (f_0) results in oil-in-water type slug flow at lower superficial gas velocity and the phase inversion of liquids moves to lower (f_0) for high superficial velocity of gas.

With the above considerations, the present study reports extensive experiments to understand the interfacial configuration during gas–liquid–liquid upflow through a vertical pipe. The optical probe technique (Jana et al.[16]), which has been reported to be successful for liquid–liquid and gas–liquid cases has been adopted for an objective identification of flow patterns during three-phase upflow. The nature of the probe signals and the probability density function (PDF) analysis of the random signals have been exploited to understand the flow distribution. The device is particularly useful at high phase velocities where visualization fails. The information leads to an online pattern detection algorithm. Further attempts have been made to propose suitable representations of flow pattern map for three-phase systems.

Experiments

General information

A schematic of the experimental setup is shown in Figure 1. It comprises of fluid handling devices (compressor, pump, flow meters, and storage tanks), test section, and separator. The setup is a vertical transparent Perspex tube of 0.0254-m diameter and 5.5-m length. Perspex (polymethyl methacrylate) has been selected as the tube material to enable visualization and photographic studies of the flow phenomenon and also to facilitate optical measurements. The test liquids are water ($\rho = 1000$ kg/m^3, $\mu = 0.001$ Pa s, $\sigma = 0.072$ N/m at 27°C), kerosene ($\rho = 787$ kg/m^3, $\mu = 0.0012$ Pa s, $\sigma = 0.027$ N/m at 27°C), and air ($\rho = 1.167$ kg/m^3, $\mu = 0.0000198$ Pa s at 27°C) and the respective range of superficial velocities in the present experiments are 0.03–0.99, 0.03–0.66, and 0.03–2 m/s. Green-dyed kerosene has been used for better visualization of the flow distribution and to ensure a wide difference in optical properties from air and water. The three phases enter the test rig through a specially designed nozzle. All the measurements are made after an entry length of 2.5 m ($L/D = 98$) to ensure fully developed flow. The liquids after the test section enter the separator where the liquids are gravity separated and recycled to their respective storage tanks while air escapes to the atmosphere.

The experiments are initially conducted at a low velocity of water. Keeping the water velocity constant, either the kerosene or the air velocity is increased from a low to a high value. The signals are recorded at each combination of phase velocity for a period of 40–60 s while the interfacial configurations are observed visually and photographed. After the signals are recorded for the entire range of both oil and air velocity, the water flow rate is increased to a higher value. This is repeated for 20 different water velocities. For each water velocity, kerosene flow is set at 20 different values. For constant water and kerosene flow rates, the air flow is varied and flow patterns are recorded.

Visualization studies

The flow patterns have been observed visually and photographed by a digital camera (DSCH9, SONY). A movable rectangular glass view box is attached to the visualization section of the test rig to eliminate the effects of refraction and reflection by the circular pipe cross section. The studies reveal that the flow configurations can grossly be categorized as water continuous and oil continuous patterns. However, only visual studies do not provide complete details regarding the distribution of the dispersed phases in the continuous medium. The technique is observed to be particularly limiting under high mixture velocities and in the oil continuous regime. Even at low flow rates, it is difficult to demarcate the transitions between successive patterns from visualization alone.

Optical probe technique

Further attempts have been made to devise a suitable technique for identifying flow patterns over a wide range of flow velocities. The technique should be based on a physical property, which is distinctly different for the three phases. A nonintrusive, low-cost device capable of instantaneous response with a good spatial resolution is preferable. The optical probe technique proposed by Jana et al.[17] is adopted. It has been shown to be useful for flow pattern identification in liquid–liquid and gas–liquid systems. Hamad et al.,[18] Chakrabarti et al.,[19] Jana et al.,[16,17] Mandal et al.,[20,21] and the present study extends the applicability of the probe for three-phase gas–liquid–liquid cases.

The probe is composed of a point semiconductor laser source ($\sim$2 mW, $\sim$660 nm, wavelength and 2 mm beam diameter) and a photodiode detector (SD 3410, manufactured by Honeywell), which generates a DC voltage when light is incident on it. The source and detector are at the same level on two limbs of a U-shaped perspex block (tuning fork type arrangement) that fits into the fluid carrying conduit and can be fixed on the pipe by a screw arrangement.

The output from the detector depends on the intensity of light incident on the photodiode. In case of single-phase flow of air, water, and kerosene, these were noted to be 8.1, 7.9, and 2.2 V, respectively. The variation between air and water is small as both fluids are colorless and transparent showing only a small difference in attenuation while colored kerosene with much higher attenuation shows a lower voltage. During multiphase flow, the output voltage, which is a function of the intensity of light incident on the photodiode, is affected by the attenuation by the medium. The scattering at the interface also influences the output signal. The interfacial configuration (liquid droplets, gas bubbles, and wavy interfaces) decides the flow patterns.

It may be noted that the effect of refraction, including total internal reflection at the interface of the bubbles/droplets will attenuate the intensity of the laser beam unless the interface surface is perpendicular to the path of the laser beam. This attenuation due to the randomness of the interface orientation is unavoidable and inherent to the system and flow pattern. In fact, this is a common limitation for any radiation attenuation technique. This effect has been minimized (a) using a point semiconductor laser source, which emits a beam of 2-mm diameter and (b) placing the source and detector in a tuning fork type arrangement to ensure that they are located diametrically opposite to each other (Figure 1). Further, we recall that the probe is used for qualitative estimation of flow pattern and no quantitative inference is drawn from the output signals. As a result, light refraction at the interface does not affect the results significantly.

The main advantage of the device is the nonintrusive nature of the probe. This has nullified the problems
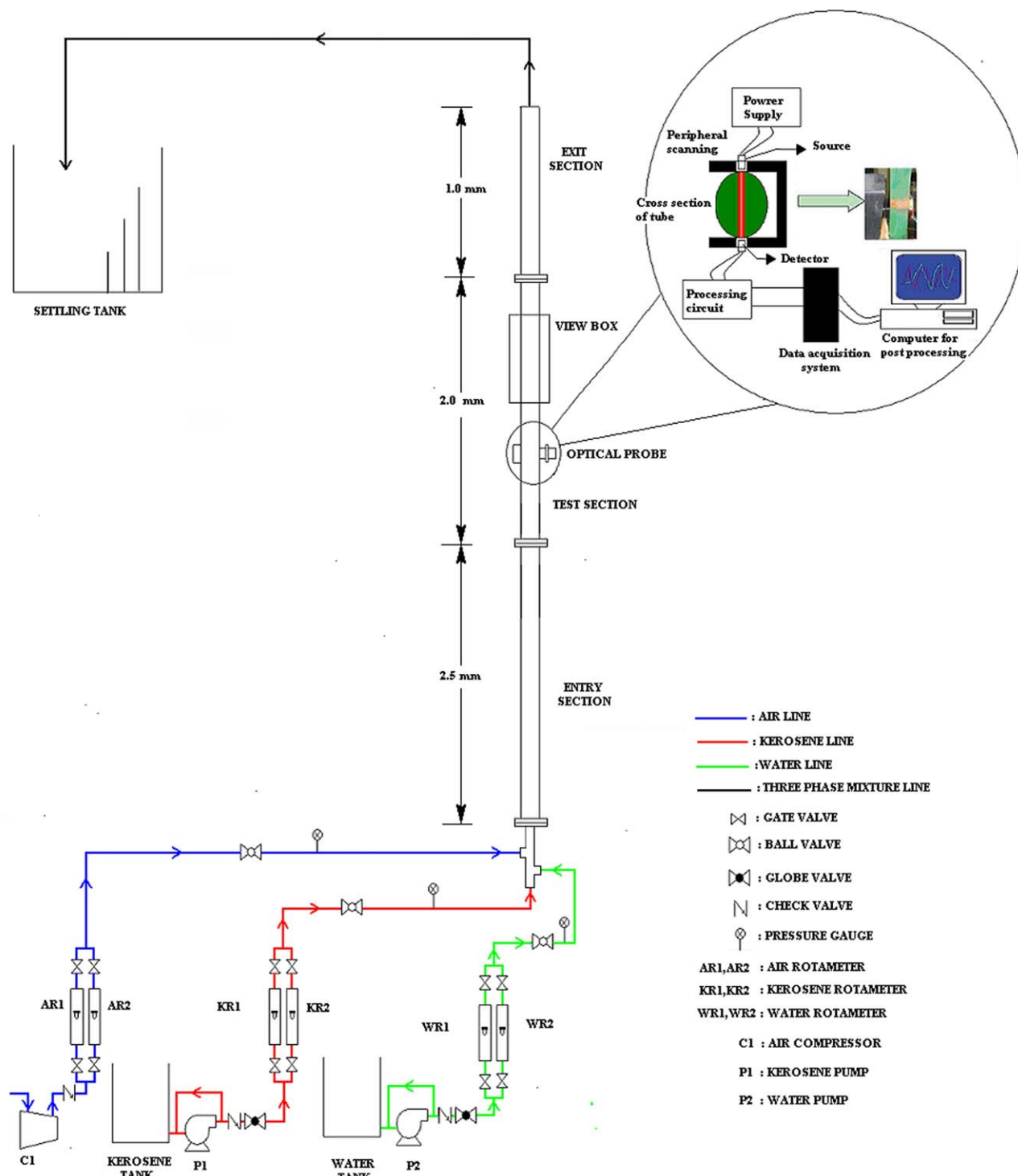
Figure 1. Schematic of experimental setup.

[Color figure can be viewed in the online issue, which is available at wileyonlinelibrary.com.]

associated with obstruction to the flow passage or wetting of the probe by the oil phase. Moreover, the device has operated both under water continuous and oil continuous flow patterns during liquid–liquid flow experiments, and therefore, is expected to elucidate flow pattern information over a wide range of flow conditions during three-phase flow. It is reliable and inexpensive. The coherent character of the laser light enables a better penetration through the fluids and a high sensitivity of the photodiode makes the response of the system extremely fast. Therefore, the device provides an instantaneous response as well as a good spatial resolution. It is small in size, easy to handle and use, and the components required are easily available. It is based only on the difference in optical properties of the fluids.

The applicability of the device is limited by the requirement of (1) a transparent pipe wall or a pair of transparent windows on it and (2) difference in transmittance between the phases and nonopacity of the phases. For example, it cannot be used to identify flow patterns if lubricating oil is used instead of kerosene.
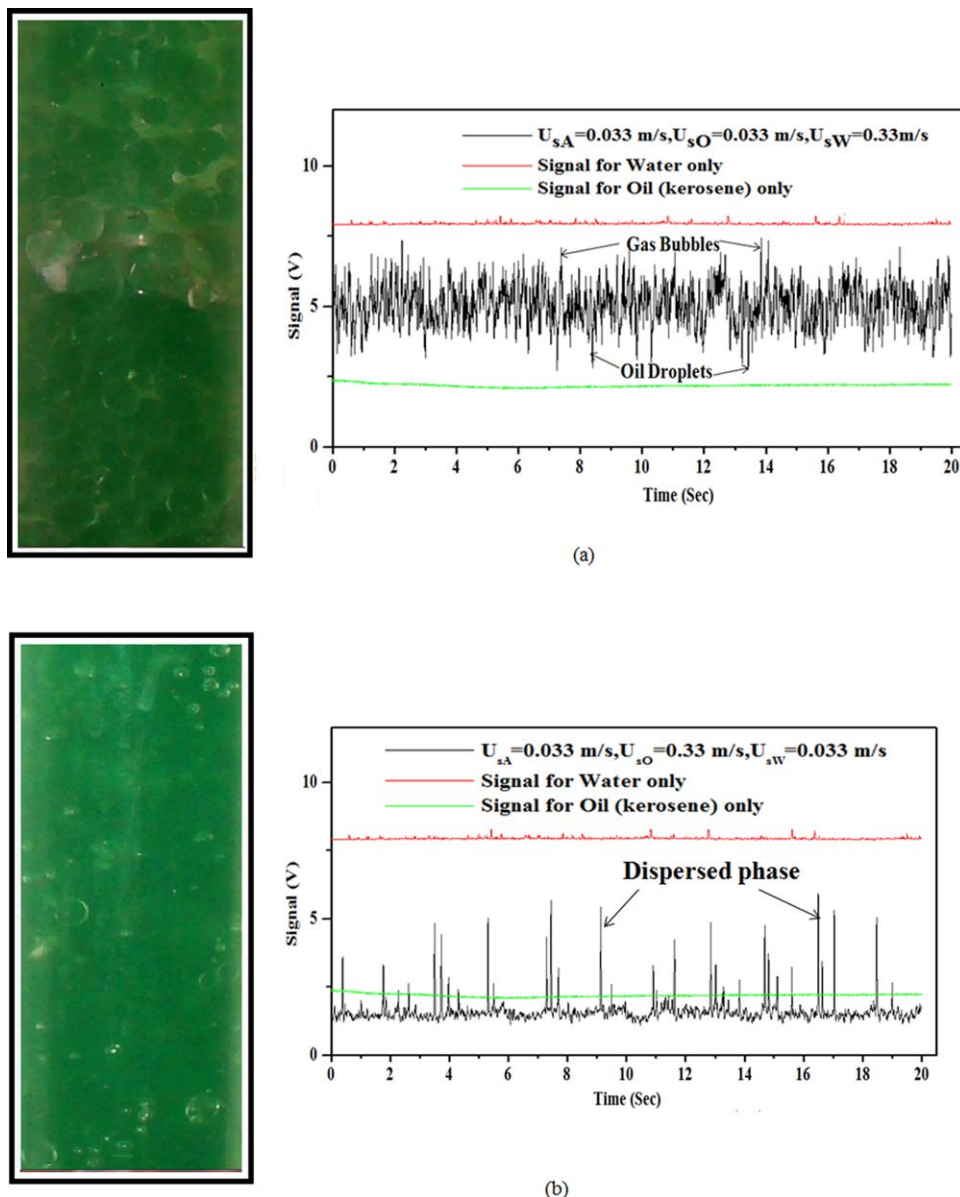
Figure 2. Optical probe signal characteristics along with photographs.

[Color figure can be viewed in the online issue, which is available at wileyonlinelibrary.com.]

A survey of the past literature reveals that the most commonly used optical technique in two- and three-phase flows is the optical fiber probe (Piela et al.,[10] Fordham et al.[22–24]). It is based on either Fresnel reflectivity or total internal reflection of light emitted from the fiber tip and is a measure of the refractive index contrast. In general, such probes fail to detect phase elements, which are small or get deflected by the probe tip. Further, the intrusive nature disturbs the flow phenomenon inside the test section. In addition, during liquid–liquid or gas–liquid–liquid flows, the wetting phase tends to stick to the probe tip and this is the most serious limitation of the device for multiphase systems. The present optical probe does away with the aforementioned limitations due to its nonintrusive nature. It can also identify small fluid elements due to scattering of light at the interface. The past researchers working with fiber optic probe have reported (Fordham et al.[24]) that for three-phase flows, a single sensor often fails to discern the three-phase distribution and a combination of dual sensors is necessary to distinguish gas–liquid and "oil–not oil" components of the mixture. In the present study, we have used a single probe to identify the flow patterns for water predominant, oil predominant, and air predominant flow conditions. We also note that the optical fiber sensor has been used primarily for dispersed three-phase flows while the present probe has been observed to be effective over a wide range of flow conditions encompassing several flow distributions.

Typical probe signals

Figures 2a, b shows the voltage signals for two cases—the first with predominantly water (80%) along with small flows of air (10%) and oil (10%). The superficial velocities are 0.33, 0.033, and 0.033 m/s, respectively. In Figure 2b, the signals are recorded with the liquid velocities interchanged such that the flow is predominantly oil (80%, 0.33 m/s) and the air and water flows (10%, 0.033 m/s) being lower. The signal obtained when the predominant phase flows alone in the pipe is also recorded and superimposed in the figures for

comparison. In each case, single-phase flow is characterized by an almost straight line output with negligible fluctuations due to noise while multiphase flow is characterized by an intensely fluctuating signal. Visual observations reveal dispersed flow in both the cases with oil droplets and gas bubbles dispersed in water in Figure 2a, and water and air propagating through oil in Figure 2b. This clearly indicates that the fluctuations occur due to scattering at the interfaces formed due to the formation of gas bubbles and liquid droplets. The mean output is lower than the weighted average (7.352 and 3.36 V) of the individual single-phase flows. This suggests the role of scattering along with light absorption in the three-phase mixture. The scattering effect in Figure 2a lower the mean signal voltage ($\approx$5 V) below the weighted average value ($\approx$7.352 V) by around 32%. In case of predominant oil flow (Figure 2b), the lowering of signal of the mean output ($\approx$1.5 V) is even below that of oil flowing as a single phase ($\approx$2.2 V). The significantly higher scattering effect in the second case (Figure 2b) can be attributed to the higher refractive index of kerosene as compared to water. Due to this, the incident rays at the water droplet or air bubble interface get scattered by a larger angle. A close observation of the figures further reveals that the signal in case of predominantly water flow (Figure 2a) shows both positive and negative spikes. These are possibly contributed by the higher transmittivity of air and lower transmittivity of oil as compared to water. In case of predominant flow of oil (Figure 2b), long spikes appear mostly above the average signal value contributed by air and water as both of these have significantly higher transmittivity than oil. It may be noted that while in Figure 2b air bubbles and oil droplets can be distinguished from positive and negative spikes, such a distinction is not possible in oil dominant flow (Figure 2b) since both air and water having higher transmittivity than oil and contributes to positive spikes. Nevertheless, a distinction between dispersed and continuous phase is possible in both the cases.

The output signal, thus, depends on the phase content as well as the interfacial configuration characterizing a particular flow pattern. Although the interfacial configuration varies in space and time, the nature of variation of the signal gives an insight into the nature of flow across a diametral plane without affecting it.

Based on the aforementioned observation, it is felt that the flow regimes can be better differentiated by normalized rather than absolute signals. Accordingly, the signals have been represented as

$$V^* = \frac{V - V_{\text{oil}}}{V_{\text{water}} - V_{\text{oil}}} \qquad (1)$$

V^*, V_{water}, V_{oil}, and V are the normalized voltage and mean signals for water only, oil only, and three-phase flow, respectively.

The PDF analysis of the signals provide a better appraisal of the flow phenomenon and the statistical moments have been used to identify the transition between different flow patterns. The physical significance of the moments in relation to the various flow patterns have been provided by Vince and Lahey[25] for gas–liquid flow and used extensively by Chakrabarti et al.[19] and Jana et al.[17] for identification of liquid–liquid flow patterns.

During initial trials with varying duration of the sampling window, we found that a sampling duration of 30 s and

above does not significantly alter the nature of the PDF curves and the quantitative measure of the PDF moments extracted from the signal sample. Therefore, the results reported are with sampling window of 40–60 s.

Results and Discussion

The results for a few representative cases have been discussed in the following section and are presented in Figures 3 and 4. In Figure 3, the PDF analysis of the probe signals have been presented along with schematic of visual observations at low phase velocities. The inferences are used to derive the flow configurations under conditions where visualization fails. The results for such cases have been depicted in a similar fashion in Figure 4. The individual rows denoting the flow situation for a particular combination of phase velocities have been numbered as Figures 3.1, 3.2, and so forth while the three columns for schematic, normalized signal, and PDF have been numbered as a, b, and c. The mean, standard deviation, peak position, skewness, and ratio of two peaks of the PDF have been denoted as m, σ, PP, S, and peak ratio in the figures. The peak position suggests the predominant phase and the mean provides an idea about the average value of distribution with the variance being a measure of the distribution about the mean. In all the figures, U_{sW}, U_{sK}, and U_{sA} refer to the respective superficial velocities of water, kerosene, and air.

Nature of flow from visualization and PDF characteristics

For low flow rates of kerosene and air at moderate flow rate of water, visualization techniques reveal a dispersion of kerosene and air in water (Figure 3.1a). Kerosene is dispersed as discrete droplets while air appears either as cap or irregular shaped bubbles. The probe signal displays oscillations with spikes directed toward both higher and lower values of V^* about a mean of 0.5. This confirms dispersion of kerosene and air in the continuous water phase and is further corroborated by a spread out unimodal PDF with PP at 0.5 and m at 0.49. The distribution has been named water continuous dispersed flow taking a cue from the nomenclature used for two-phase flows.

An increase in water velocity at constant kerosene and air flow (Figures 3.2 and 3.3) is characterized by a similar visual appearance and is marked by a similar unimodal PDF, which exhibits a slight increase in the mean and peak signal while the spread remains relatively unaffected ($\sigma \sim 0.12$). Similarly, an increase in oil velocity does not have a significant effect on the PDF characteristics except shifting the mean and PP to slightly lower values (Figures 3.4 and 3.5). Interestingly, a close observation reveals an increase in water velocity results in a slight shift of skewness to a lower value while the reverse occurs for increased oil flow. This probably arises due to an increased frequency and size of oil droplets in the former case and a preponderance of air bubbles in the latter case.

An increase in air flow brings about an increase in the size of the cap bubbles and leads to the formation of axisymmetric bullet-shaped Taylor bubbles (Figure 3.6a) commonly observed for gas–liquid flows. Under this condition, the flow distribution assumes the periodic characteristic of slug flow with air Taylor bubbles alternating with liquid slugs and is characterized by bimodal PDF (Figures 3.6b and 3.6c) in agreement to the common observation during gas–liquid slug
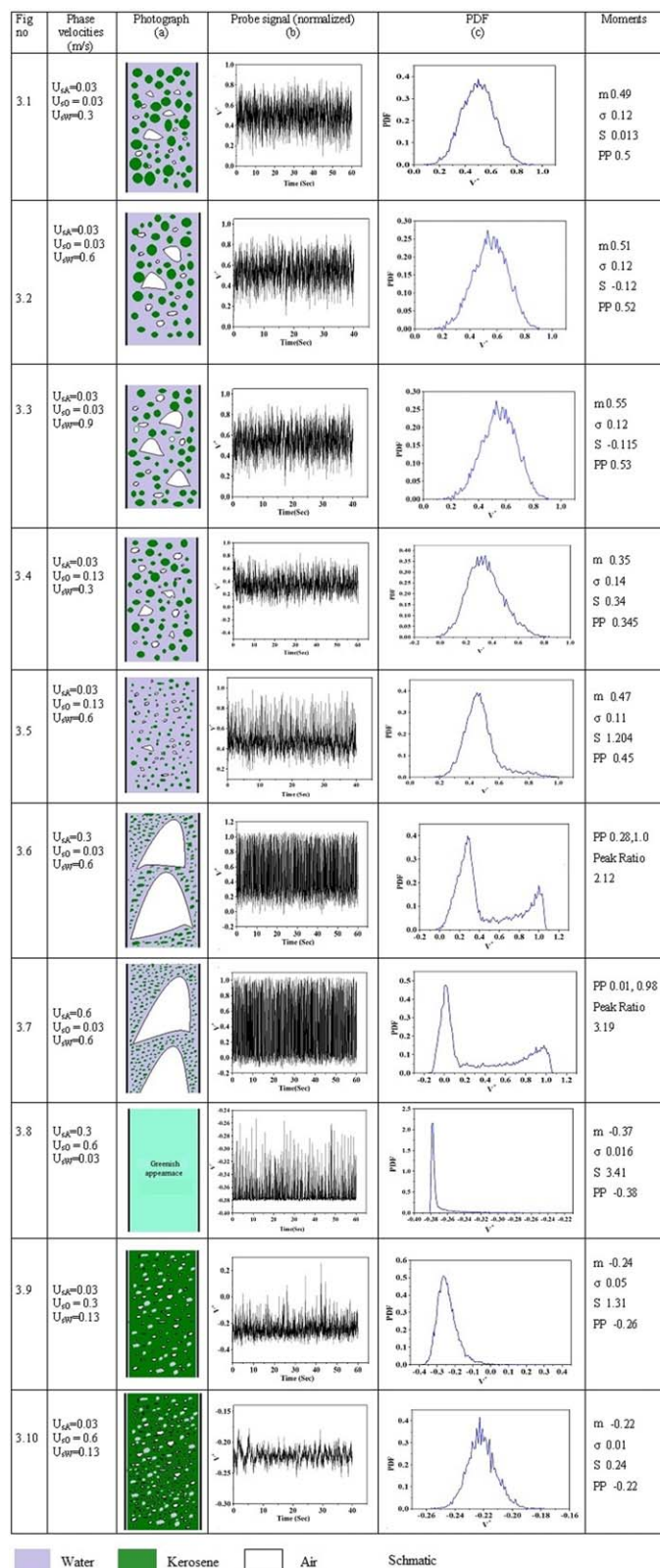
Figure 3. Schematic, probe signal, PDF curve for the flow pattern at low phase velocities.

[Color figure can be viewed in the online issue, which is available at wileyonlinelibrary.com.]

flow. Visualization reveals liquid slugs to contain oil dispersed in water and this explains the position of the low voltage peak between 0 and 0.5.

As we increase air velocity further (Figure 3.7), the PDF remains bimodal with the low voltage peak shifting to still lower V^* (preponderance of dispersion) while the high voltage peak exhibits a similar PP and is accompanied by increase in the ratio of the low to high voltage peak (peak ratio in the figures). This suggests that an increase in air velocity in the slug flow pattern causes an increased
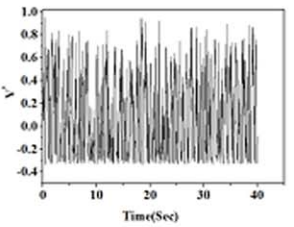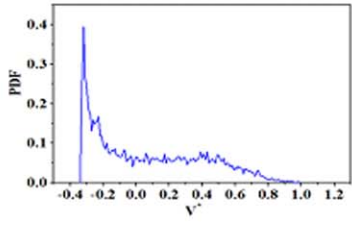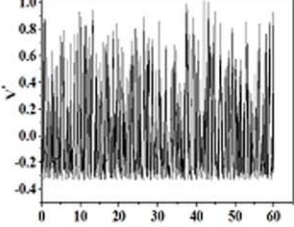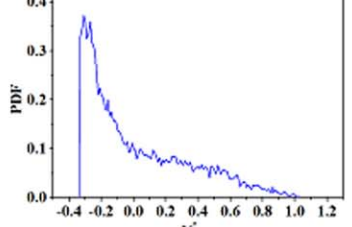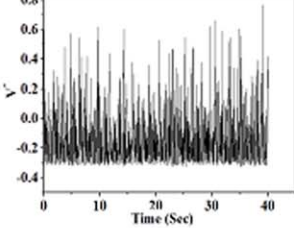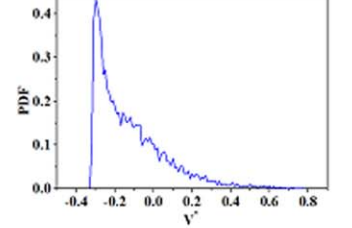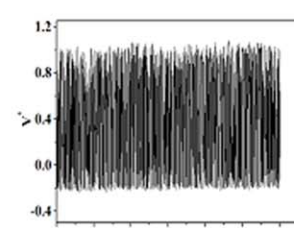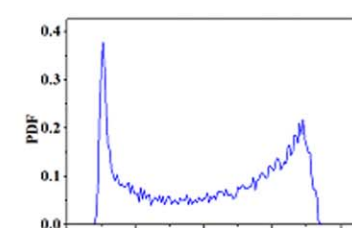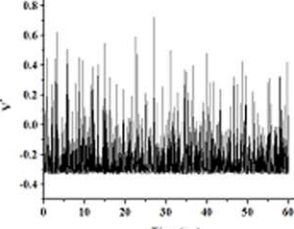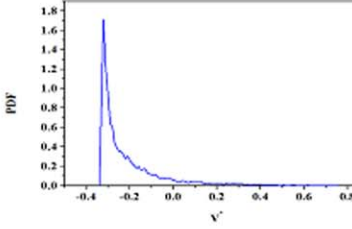
Fig no	Phase velocities (m/s)	Photograph (a)	Probe signal (b)	PDF (c)	Moments
4.1	$U_{sA}=1.31$ $U_{sO}=0.03$ $U_{sW}=0.03$	Greenish appearance			m 0.07 σ 0.33 S 0.48 PP -0.32
4.2	$U_{sA}=2$ $U_{sO}=0.03$ $U_{sW}=0.03$	Greenish appearance			m 0.02 σ 0.31 S 0.94 PP -0.31
4.3	$U_{sA}=2$ $U_{sO}=0.6$ $U_{sW}=0.6$	Greenish appearance			m -0.12 σ 0.17 S 1.345 PP -0.3
4.4	$U_{sA}=2$ $U_{sO}=0.03$ $U_{sW}=0.6$	Greenish appearance			PP -0.19,0.96 Peak Ratio 1.79 M 0.447
4.5	$U_{sA}=2$ $U_{sO}=0.6$ $U_{sW}=0.03$	Greenish appearance			m -0.2174 σ 0.141 S 2.277 PP -0.32

Figure 4. Schematic, probe signal, PDF curve for the flow pattern at high phase velocities.

[Color figure can be viewed in the online issue, which is available at wileyonlinelibrary.com.]

dispersion in the liquid slugs rather than an increase in the length of the Taylor bubbles for the flow conditions investigated. Possibly the turbulent energy dissipated to the liquid mixture under slug flow is sufficient not only to attain a dispersion of oil in water but also to maintain air dispersion in the liquid slugs. Nevertheless, most of the air remains as elongated bullet-shaped sections between successive liquid slugs. The configuration characterized by a bimodal PDF with the two peaks positioned at $0 < V^* < 0.5$ and ~ 1.0 has been termed as the water continuous slug flow pattern.

On interchanging the individual liquid velocities for the same air flow, we note a completely different visual
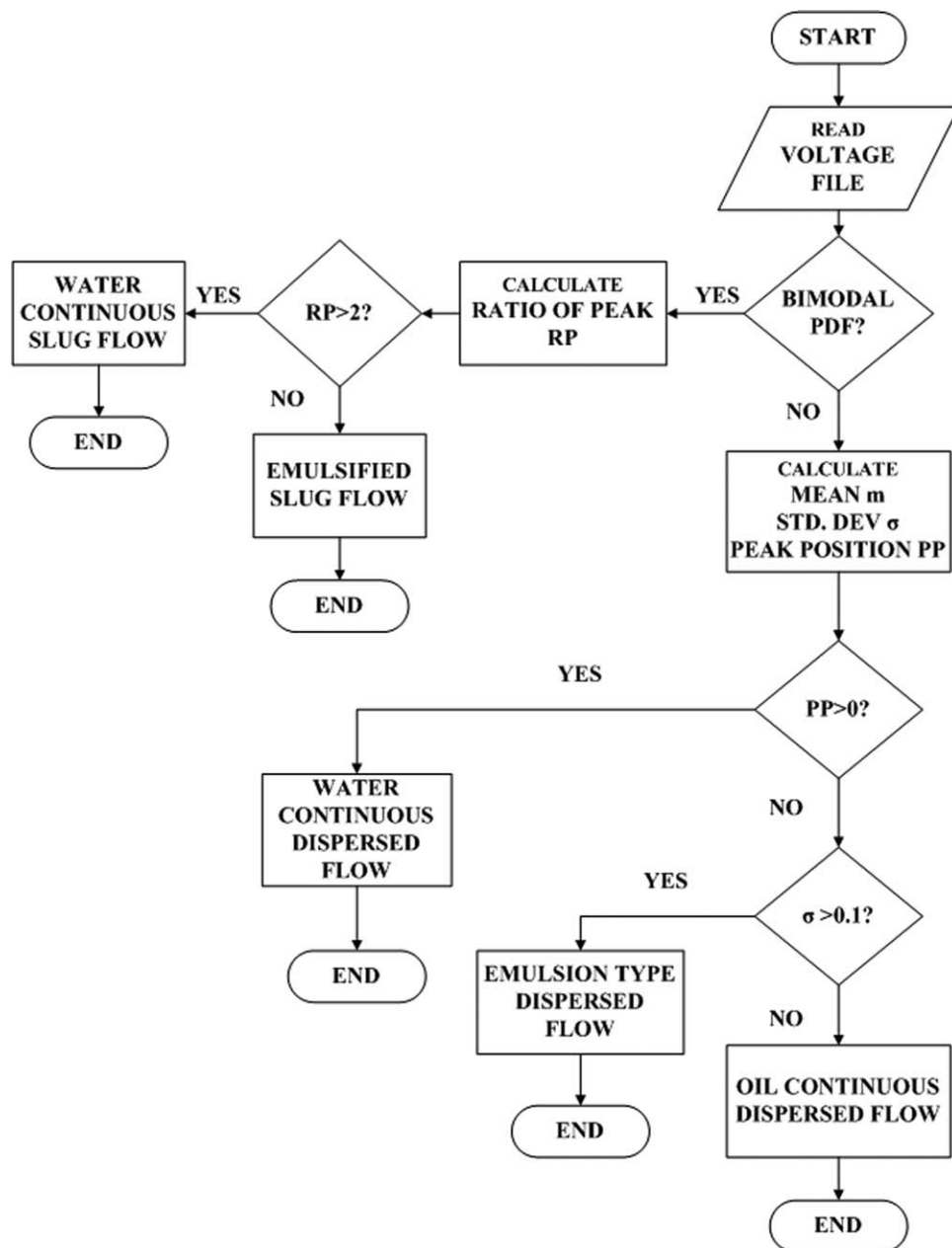
Figure 5. An algorithm for detection of flow patterns.

appearance (Figure 3.8). The flow assumes a uniform greenish appearance and the individual phases can no longer be distinguished. The corresponding PDF curve is unimodal with the mean and PP being less than zero. It exhibits a large positive skewness and a significant reduction in PDF spread. A comparison with the unimodal PDFs reported in Figures 3.1–3.5 suggests dispersed flow with oil as the continuous phase. However, further investigations are necessary to confirm the supposition and a detailed discussion in this regard is provided in the next section.

For low velocities of water and air and moderate to high velocities of kerosene, the flow passage appears green with patches of air and droplets of water dispersed in it. The corresponding probe signal and PDF curve is depicted in Figure 3.9. The unimodal PDF confirms dispersed flow and the peak at negative V^* confirms kerosene to be the continuous

phase. This has been named oil continuous dispersed flow and can be distinguished from the water continuous situation by the mean and peak position being less than zero in the present case and greater than zero ($V^* \sim 0.5$) in the former situation. A further increase in oil velocity causes a homogenized green appearance with uniform dispersion of colorless bubbles and droplets (Figure 3.10). A comparison with Figure 3.9 indicates an abrupt decrease of the PDF skewness to less than unity while the mean, peak position, and spread remains relatively unaffected. This is indicative of an increase in the kerosene phase and a predominance of attenuation over scattering by the flowing mixture. Accordingly this also corresponds to oil continuous dispersed flow.

We note that Figures 3.5 and 3.10 have been reported with the liquid velocities interchanged for constant air flow. Figure 3.5 shows air existing as cap bubbles or oblate
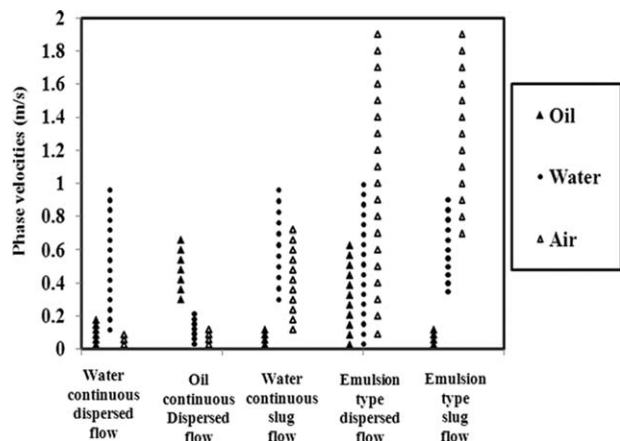
Figure 6. Three-phase flow pattern map on Cartesian coordinate.

spheroids, while in Figure 3.10 water and air are finely dispersed in oil. We recall that Chakrabarti et al.[19] could distinguish phase inversion in two-phase liquid–liquid flow by a shift in the sign of the skewness. However, we do not observe such a feature in three-phase flow probably due to the presence of the air phase.

Flow distribution at high air velocities

At high air velocity ($U_{sA} > 1$ m/s), we observe a uniform greenish white appearance of the flow passage under all flow conditions. The intensity of color seems to change with flow conditions but no additional information can be obtained from visualization. The PDF for low liquid velocity (Figure 4.1) is unimodal with the peak being located at negative V^* and the curve spreads over the entire range of V^* unlike the dispersed flow PDFs in Figure 3. This has resulted in a large standard deviation ($\sigma > 0.3$). Another unique feature marks the present unimodal PDFs. We note that the mean is significantly different from the peak position, whereas in Figure 3, the mean and peak positions were always observed to be close to each other for dispersed flow. Both were located between 0.3 and 0.5 when water was the continuous phase and were either negative or slightly positive for the oil continuous distribution. All these suggest that the flow situations represented in Figure 3 had a preponderance of one of the phases while at high air velocities, the position of the peak (at a negative V^*) arises primarily due to scattering. This

Figure 7. Three-phase flow pattern map on triangular coordinate.

hints at an emulsified flow situation with all the three phases fairly well mixed and none serving as the continuous or the dominant phase. In fact, the distinctly different visual appearance of the PDFs brings out the difference in distribution as compared to the dispersed distribution presented in Figure 3. Following the nomenclature proposed by Wang et al.[4], the flow pattern is termed as emulsion type dispersed flow.

An increase in air velocity (Figure 4.2) causes a slight shift of the mean to a lower V^* and a broadening of the area under the curve. This further confirms that the increased air contributes to increased scattering of the laser beam. Nevertheless, the PDF moments namely mean, peak position, and spread remains relatively unaltered showing that the gross characteristics of the pattern is not significantly affected by the higher air velocity. An increase in total liquid velocity while maintaining the same proportions of oil and water (Figure 4.3) results in a further shift of the mean to lower V^* (negative V^*) accompanied by a decrease in the standard deviation and an increase in the skewness. This hints at the fact that the emulsion assumes a more homogeneous nature at higher liquid velocities.

We also note that an increase in water velocity at constant oil and air flow (Figure 4.4) results in a bimodal PDF. This is indicative of the fact that at increased water velocity, air dominant and liquid dominant zones are formed. The PDFs do not provide any information regarding the shape of the air plugs and it cannot be said whether air assumes the typical bullet shape characterizing Taylor bubble. Nevertheless, the position of the high voltage peak close to unity and a low voltage peak at $V^* < 0$ suggests that the flow distribution is periodic. Hence the flow pattern is termed emulsion type slug flow and can be distinguished from water continuous slug flow by the position of the low voltage peak, which is positive for the former case and negative in the present situation. The peak ratio has also been observed to be less as compared to water continuous slug flow.

Interestingly, an interchange of the liquid flow rates at constant air velocity results in disappearance of the high voltage peak (Figure 4.5). The resulting PDF is unimodal with a peak position ~ -0.3 similar to that obtained in Figures 4.1–4.3. It also exhibits a decreased mean and a reduced spread. This is probably due to enhanced attenuation by the higher oil fraction in the pipe. Several such experiments show slug flow to occur at high water and air velocity. However, at high oil flow, the increased air velocity causes a greater dispersion but never leads to the formation of cap or Taylor bubbles. We recall that similar results had been reported in Figures 3.6 and 3.8 for a lower air and the same liquid velocities.

Flow pattern detector from PDF moments

Based on the aforementioned discussion, the flow patterns identified by the optical probe technique are (1) water continuous dispersed flow at moderate to high water velocity and low air and kerosene flow, (2) water continuous slug flow at higher air velocities, (3) oil continuous dispersed flow at higher oil velocities, (4) emulsion type dispersed flow at higher air velocities, and (5) emulsion type slug flow for high water and air velocities. The distributions have been distinguished by the number of peaks, mean, and peak position(s) as well as the standard deviation. Interestingly, these moments do not change significantly with change in phase
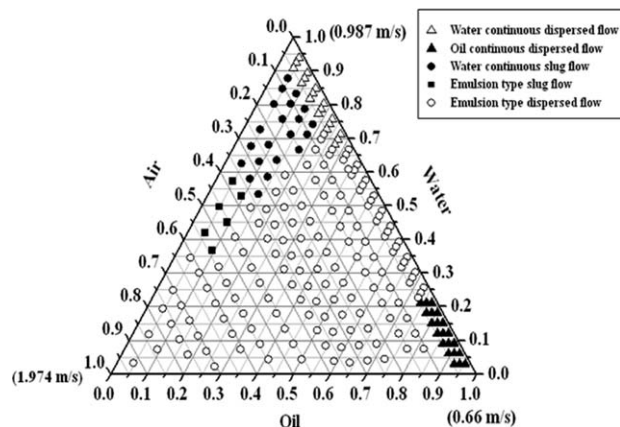
flow rates within a particular flow pattern but exhibit a distinct change during transition. A summary of the PDF characteristics identifying the different patterns are listed in Table 2.

The table reveals that dispersed flow generates a unimodal PDF whereas for slug flow it is bimodal in nature. Further, water and oil continuous dispersed flow can be distinguished by the mean and peak position(s) being greater than 0.3 for water continuous dispersed flow and less than zero for the oil continuous case. Emulsion type dispersed distribution has a distinctly different appearance of the PDF. It is characterized by a large spread ($\sigma > 0.1$) and the value of mean (lying between -0.1 and 0.1) being significantly different from the peak position (< -0.3). The high standard deviation indicates dense dispersion and the low mean is attributed to scattering rather than attenuation of light in contrast to the observation for the oil continuous pattern. Water continuous and the emulsion type slug flow can be easily distinguished by the position of the low voltage peak of the bimodal PDF. The high voltage (V^*) peak lies close to 1 in both cases. The position of the low voltage (V^*) peak is positive for the water continuous case and is negative for the emulsion type flow. Further, a close observation of experimental data reveals that for emulsion type slug flow the peak ratio is greater than 2 while it less than 2 for the water dominant regime.

From the above inferences, an algorithm is developed for detection of flow patterns using the PDF moments of the optical probe signals as the input. The algorithm is presented as a flowchart in Figure 5. The inferences based on the qualitative nature of the signal are general but the numerical values of the parameters used in the algorithm are specific to this setup.

Flow pattern map

Flow patterns in three phase is governed by the superficial velocities/flow rates of the individual phases as well as the total velocity/flow in the conduit. A survey of the past literature shows that for three-phase flow, two dimensional flow pattern maps are constructed based on flow parameters of any two phases keeping the corresponding parameter of the third phase constant. The flow parameters selected by the different researchers are either superficial velocities (volumetric flux) or volume fraction of the individual phases (Wang et al.,[4] Ackigoz et al.,[5] Stapelberg et al.,[6] Wegmann et al.,[8] Chen et al.,[12] Oddie et al.[13]). This approach requires several maps/plots to show the patterns in the entire range of flow.

In the present study, two representations to identify the range of existence of the different flow patterns as a function of three-phase flow velocities has been attempted.

The first approach presents the range of phase superficial velocities for each of the five flow patterns (Figure 6). The prevailing flow pattern for different combinations of velocities can be detected by noting the pattern cluster, which contains each of these phase velocities.

Three different symbols have been used to depict the flow patterns inferred from the probe signals. From the figure, it is evident that the flow is air dispersed in liquid at low air velocities (0.03–0.1 m/s). The continuous phase is decided by the individual liquid velocities and the distribution is water continuous for water velocities greater than 0.1 m/s and oil continuous for oil velocities above 0.3 m/s. At

Table 2. Summary of PDF Characteristics for Different Flow Patterns

Flow Pattern	Nature of PDF	Mean m	Peak Position (PP)	Peak Ratio (PR)	Standard Deviation (σ)	Skewness (S)	Brief Comments
Water continuous dispersed flow	Unimodal	0.3–0.7	0.3–0.7	–	0.05–0.2	–0.1 to 0.4	Mean and peak position very near to one another. Skewness decreases with water velocity
Oil continuous dispersed flow	Unimodal	<0	<0	–	<0.1	0.1–2.0	Mean and peak position close to one another. Skewness decreases with kerosene velocity
Emulsion type dispersed flow	Unimodal	(−0.1)–(0.1)	<(−0.3)	–	>0.1	0.2–3.0	Mean and peak position far apart
Water continuous slug flow	Bimodal	0.3–0.7	Low voltage peak: >0; High voltage peak: >0.9	>2	Not relevant	Not relevant	Low voltage side peak position depends on kerosene as well as air velocities.
Emulsion type slug flow	Bimodal	0.3–0.5	Low voltage peak : <0; High voltage peak: >0.9	<2	Not relevant	Not relevant	Low voltage side peak position depends only on kerosene velocity.

constant water velocity (say 0.3 m/s), water continuous slug flow appears for moderate air velocity (>0.3 m/s) and low kerosene velocity (<0.2 m/s). An increase in air velocity causes the flow to become emulsion type in nature irrespective of the liquid velocity. Further, although emulsion type dispersed flow is more common at high air velocity for all combinations of water and kerosene velocity, emulsion type slug flow appears beyond a critical water velocity for low kerosene flow.

The second approach is developed taking a cue from conventional two-phase flow pattern maps that use the superficial velocities in Cartesian coordinate as the axes. It is felt that a ternary flow pattern map for three-phase flows would be useful. Accordingly, the flow pattern map (Figure 7) has been developed with the axes (scaled from 0 to 1) representing the normalized phase superficial velocities. The maximum velocity of the corresponding phase in the entire experimental range is used for normalization. Each point on the diagram thus represents a combination of phase superficial velocities. Five symbols have been used to depict flow patterns in this case. A close observation of the plot reveals that on moving away from extreme right vertex (corresponding to maximum oil velocity) to closer to the top vertex (corresponding to maximum water velocity), the water velocity at low air (<0.1 m/s) brings about the transition from oil continuous dispersed flow to water continuous dispersed flow via the emulsified dispersed flow regime. An increase in air velocity at low kerosene velocity (say <0.1 m/s) causes a transition from water continuous dispersed flow to water continuous slug flow. Increasing air velocity beyond 0.7 m/s brings about emulsified slug flow. It is also evident that the air–liquid ratio is comparable in both water continuous and oil continuous dispersed flow whreeas for emulsified flow it is higher. The oil fraction in liquid for water continuous dispersed and water continuous slug flow are comparable. Thus, we note that the ternary plot enables us to trace the path of phase inversion as well as the transition between flow patterns.

It may be noted that the ternary plot is possible only for velocity combinations, which satisfy the condition of triangular coordinate and accordingly, it cannot be extended for the entire range of three-phase superficial velocities. However, the other approach (Figure 6) does not suffer from such a limitation.

Conclusions

The present study adopts the PDF analysis of the optical probe signals to infer the flow patterns during gas–liquid–liquid three-phase upflow through a pipe. The technique is noted to be more effective than the existing optical techniques reported in literature.

The PDF moments as obtained from the probe signals have enabled the identification of the flow patterns over a wide range of flow conditions including water dominant, oil dominant, and air dominant flow conditions. Online processing of the probe signals with the suggested algorithm can be exploited to identify the prevailing flow pattern in three-phase upflow. The transition between consecutive flow patterns can also be traced.

The flow pattern maps have been represented in the form of a ternary plot and also by a bar graph. While the ternary plot elucidates flow pattern transitions, the bar graph representation can be used over the entire range of phase velocities.

Though the probe signal analysis and the novel representations of flow patterns has been performed specifically for air–kerosene–water upflow in this work, the same can be extended to other situations of three-phase flow provided the phases have different optical property and a fair degree of transmittance. In the light of the fact that estimation of flow pattern is not easy even for two-phase flow, the present study appears to be a fruitful endeavor for gas–liquid–liquid three-phase systems.

Acknowledgment

Literature Cited

1. Woods GS, Spedding PL, Watterson JK, Raghunathan RS. Three-phase oil/water/air vertical flow. *Chem Eng Res Des.* 1998;76:571–584.
2. Descamps M, Oliemans RVA, Ooms G, Mudde RF, Kusters R. Influence of gas injection on phase inversion in an oil-water flow through a vertical tube. *Int J Multiphase Flow* 2006;32:311–312.
3. Descamps MN, Oliemans RVA, Ooms G, Mudde RF. Experimental investigation of three-phase flow in a vertical pipe: local characteristics of the gas phase for gas-lift conditions. *Int J Multiphase Flow* 2007;33:1205–1231.
4. Wang ZY, Jin ND, Gao ZK, Zong YB, Wang T. Nonlinear dynamical analysis of large diameter vertical upward oil-gas-water three phase flow pattern characteristics. *Chem Eng Sci.* 2010;65:5226–5236.
5. Acikgoz M, Franca F, Lahey RT. An experimental study of three phase flow regimes. *Int J Multiphase Flow* 1992;18:327–336.
6. Stapelberg HH, Mewes D. The pressure loss and slug frequency of liquid-liquid-gas slug flow in horizontal pipes. *Int J Multiphase Flow* 1994;20:285–303.
7. Spedding PL, Donnelly GF, Cole JS. Three phase oil–water–gas horizontal co-current flow: experimental and regime map. *Chem Eng Res Des.* 2005;83:401–411.
8. Wegmann A, Melke J, Rohr PRV. Three phase liquid-liquid gas flows in 5.6 mm and 7 mm inner diameter pipes. *Int J Multiphase Flow.* 2007;33:484–497.
9. Bannwart AC, Rodriguez OMH, Trevisan FE, Vieira FF, Carvalho CHM. Experimental investigation on liquid–liquid–gas flow: flow patterns and pressure-gradient. *J Pet Sci Eng.* 2009;65:1–13.
10. Piela K, Delfos R, Oom G, Westerweel J. Dispersed oil-water gas flow through a horizontal pipe. *AIChE J.* 2009;55:1090–1102.
11. Poesio P, Strazza D, Sotgia G. Very viscous oil/water/air flow through horizontal pipes: pressure drop measurement and prediction. *Chem Eng Sci.* 2009;64:1136–1142.
12. Chen X, Guo L. Flow patterns and pressure drop in oil-air-water three-phase flow through helically coiled tubes. *Int J Multiphase Flow.* 1999;25:1053–1072.
13. Oddie G, Shi H, Durlofsky LJ, Aziz K, Pfeffer B, Holmes JA. Experimental study of two and three phase flows in large diameter inclined pipes. *Int J Multiphase Flow.* 2003;29(4):527–558.
14. Spedding PL, Benard E, Crawford NM. Fluid flow through a vertical to horizontal 900 elbow bend III three phase flow. *Exp Therm Fluid Sci.* 2008;32:827–843.
15. Tek MR. Multiphase flow of water, oil and natural gas through vertical flow strings. *J Pet Technol.* 1961;13:1029–1036.
16. Jana AK, Mandal TK, Chakrabarti DP, Das G, Das PK. An optical probe for liquid–liquid two-phase flows. *Meas Sci Technol.* 2007;18:1563–1575.
17. Jana A K, Das G, Das PK. Flow regime identification of two phase liquid–liquid upflow through vertical pipe. *Chem Eng Sci.* 2006;61:1500–1515.
18. Hamad FA, Imberton F, Brunn HH. An optical probe for measurement in liquid–liquid two-phase flow. *Meas Sci Technol.* 1997;8:1122–1132.

19. Chakrabarti DP, Das G, Das PK. The transition from water continuous to oil continuous flow pattern. *AIChE J.* 2006;52:3668–3678.

20. Mandal TK, Bhuyan MK, Das G, Das PK. Effect of undulation on gas–liquid two-phase flow through a horizontal pipeline. *Chem Eng Res Des.* 2008;86:269–278.

21. Mandal TK, Das G, Das PK. An appraisal of liquid–liquid slug flow in different pipe orientations. *Int J Multiphase Flow.* 2010;36:661–667.

22. Fordham EJ, Holmes A, Ramos RT, Simonian S, Huang SM, Lenn CP. Multi-phase-fluid discrimination with local fibre-optical probes. I. Liquid/liquid flows. *Meas Sci Technol.* 1999;10:1329–1337.

23. Fordham EJ, Simonian S, Ramos RT, Holmes A, Huang SM, Lenn CP. Multi-phase-fluid discrimination with local fibre-optical probes. II. Gas/liquid flows. *Meas Sci Technol.* 1999;10:1338–1346.

24. Fordham EJ, Ramos RT, Holmes A, Simonian S, Huang SM, Lenn CP. Multi-phase-fluid discrimination with local fibre-optical probes. III. Three-phase flows. *Meas Sci Technol.* 1999;10:1347–1352.

25. Vince MA, Lahey RT, Jr. On the development of an objective flow regime indicator. *Int J Multiphase Flow.* 1982;8:93–124.